A thermostat-consistent fully coupled molecular dynamics – generalised fluctuating hydrodynamics model for non-equilibrium flows

*Xinjian Liu, Ivan Korotkin, Zhonghao Rao, Sergey Karabasov**

X. Liu, Z. Rao.
School of Electrical and Power Engineering, China University of Mining and Technology, Xuzhou, 221116, China

X. Liu, S. Karabasov
The School of Engineering and Materials Science, Queen Mary University of London, Mile End Road, E1 4NS London, United Kingdom
E-mail: s.karabasov@qmul.ac.uk

I. Korotkin
Mathematical Sciences, University of Southampton, University Rd., SO17 1BJ, United Kingdom

Keywords: hybrid molecular dynamics-continuum hydrodynamics methods, molecular dynamics, multiscale modeling, linearization, non-equilibrium

The thermostat-consistent fully coupled molecular dynamics – generalised fluctuating hydrodynamics method is developed for non-equilibrium water flow simulations. The model allows for strong coupling between the atomistic and the continuum hydrodynamics representations of water and shows an improved stability in comparison with the previous formulations of similar multiscale methods. Numerical results are demonstrated for a periodic nano-scale Poiseuille flow problem with SPC/E water. The computed time-averaged velocity profiles are compared with the analytical solution, and the thermal velocity fluctuations are well reproduced in comparison with the Equilibrium Molecular Dynamics (EMD) simulation. Several options to account for the long-range electrostatics interactions available in GROMACS are incorporated in the model and compared. It is demonstrated that the suggested non-equilibrium multiscale model is a factor of 4 to 18 faster in comparison with the standard all-atom equilibrium molecular dynamics model for the same computational domain size.

1. Introduction

One of the popular categories of multiscale methods for atomistic-scale resolving simulations of non-equilibrium liquid flows is based on the idea of dividing the computational domain into an overlapping region of the continuum Navier-Stokes equations and the molecular dynamics region following the pioneering work of O'Connell and Thompson [1]. In further models, more accurate continuum models of dense liquids were used such as the Landau-Lifshitz Fluctuating Hydrodynamics (LL-FH) equations [2], which also preserve thermal fluctuations thereby enabling more consistent coupling with molecular dynamics [3-5]. A finite overlap (buffer) region between the models of different resolutions is beneficial for a smooth

transition between the continuum and atomistic parts of the model to avoid sharp oscillations [6]. In multi-particle methods [7-8], such buffer region also contains a multi-resolution region where discrete particles transition from the fully atomistic to a coarse-grained representation. Consequently, the coarse-grained particles are coupled with the continuum flow models which lead to a micro-meso-macro scale formulation[8-9]. For multi-resolution fluid dynamics modelling, the coupling between the models of different resolution should respect conservation of both the mass and the linear momentum. To automatically satisfy these conservation laws, the two-phase analogy multiscale method was suggested in [10-11], which considered the continuum and atomistic representations of a liquid as phases of a nominally two-phase flow. The phases are allowed to transition one to another in accordance with a concentration field, a user-defined function that determines which parts of the computational domain need to be modelled at molecular dynamics resolution, and which do not. The continuum phase is governed by the LL-FH-type equations integrated over control volumes, which are smoothly replaced by the averaged fields obtained from the molecular dynamics equations in the region of atomistic resolution of the multiscale model. To avoid separation of the two phases in the buffer region, forcing functions are introduced in the molecular dynamics equations, which correspond to the equivalent source and sink terms in the control volume averaged mass and momentum equations. The latter equations are more complex in comparison with the LL-FH model. Hence, in a number of cases, where the effect of the molecular phase on the continuum part of the model could be included in the calibration of the constitutive relations of the continuum model, such as the equation of state, a one-way coupled model case was used. Such one-way coupled model accounted for the continuum flow effect on microscopic particles while ignoring the feedback [12-14]. Despite the relative simplicity, the one-way-coupled approach performs well for a range of problems including the diffusion of peptides in cross flow [15-16], oscillations of a PCV2 virus capsid in water [17], and the nano-confined water effects in a High-Speed Atomic Force Microscope experiment [18]. However, to achieve the full potential of the

hybrid multiscale method in terms of accuracy and computational performance, the two-way coupling of the phases is needed. To do so efficiently, the governing equations of the two-phase flow analogy model [19] were rearranged to the single set of Generalised Landau-Lifshitz Fluctuating Hydrodynamics equations (GLL-FH), implemented in GROMACS [20], and applied for liquid argon simulations [21]. In comparison with the standard LL-FH model, the GLL-FH equations are mathematically equivalent to the control-volume averaged molecular dynamics equations and reduce to the standard LL-FH equations for the pure continuum hydrodynamics phase. To extend the original model to more complex liquids such as water, the two-way coupled GLL-FH model was further extended to the local thermostat equations in Ref.[22], where the thermostat-consistent fully coupled molecular dynamics – generalised fluctuating hydrodynamics model of SPC/E water was developed. Because of the simple Langevin thermostat used, which does not preserve the linear momentum of macroscopic flow, the implementation was limited to water fluctuations in equilibrium conditions. Hence, the present work is devoted to extending the model to non-uniform flow by using a new linearisation approach, which also allows one to couple the suggested method with an external macroscopic flow model (such as Fluid-Structure-Interaction in the future). To achieve this goal, a more stable approximation of the source terms of the GLL-FH equations is developed and several formulations for simulating long-range electrostatic interactions available in GROMACS are implemented.

2. Method

2.1 Two-phase flow analogy equations and the Generalised Landau-Lifshitz Fluctuating Hydrodynamics model

Following Ref.[10], the equations of conservation of mass (1),(2) and momentum (3),(4) of the two-phase flow representative of SPC/E water are considered, where a user-defined concentration function s is introduced. The latter function enables the smooth transition of model resolution from the pure molecular dynamics zone ($s = 0$) to the pure continuum zone (s

= 1). In the intermediate buffer region ($0 < s < 1$), the two phases co-exist, which gives rise to the exchange (source/sink) terms on the right-hand-side of the phase equations:

$$\delta_t\left(sm\right)+\sum_{\gamma=1}^{6}\left(s\rho\tilde{\mathbf{u}}\cdot d\mathbf{n}^{\gamma}\right)\cdot\delta t = J_1\cdot\delta t \tag{1}$$

$$\delta_t\left(\sum_{p=1}^{N}\left[\left(1-s_p\right)m_p\right]\right)+\sum_{\gamma=1}^{6}\left(\sum_{p=1}^{N_\gamma}\left[\left(1-s_p\right)\rho_p\mathbf{u}_p\right]\cdot d\mathbf{n}^{\gamma}\right)\cdot\delta t = -J_1\cdot\delta t \tag{2}$$

$$\delta_t\left(smu_i\right)+\sum_{\gamma=1}^{6}\left(s\rho u_i\tilde{\mathbf{u}}\cdot d\mathbf{n}^{\gamma}\right)\cdot\delta t = sF_i\cdot V\delta t + J_2\cdot\delta t \tag{3}$$

$$\delta_t\left(\sum_{p=1}^{N}\left[\left(1-s_p\right)m_p u_{ip}\right]\right)+\sum_{\gamma=1}^{6}\left(\sum_{p=1}^{N_\gamma}\left[\left(1-s_p\right)\rho_p u_{ip}\mathbf{u}_p\right]\cdot d\mathbf{n}^{\gamma}\right)\cdot\delta t = \sum_{p=1}^{N}\left[\left(1-s_p\right)F_{ip}^{MD}\right]\cdot V\delta t - J_2\cdot\delta t \tag{4}$$

Here i=1, 2, 3 denotes x, y and z components, variables with and without sub-index p correspond to molecular dynamics phase and the continuum cell-volume/flux averaged values, respectively; γ corresponds to one of the six faces of the hexahedral control volume of the computational grid, V; m and ρ are the local mass and density of the continuum phase per given control volume; m_p and $\rho_p = m_p/V$ are the particle mass and its effective density per control volume, respectively; $\mathbf{u}_p$ and $\tilde{\mathbf{u}}$ correspond to particle velocity and velocity of the two phase 'mixture', which is given by $\tilde{u}_i = \left[s\rho u_i + \sum_{p=1}^{N}\left[\left(1-s_p\right)\rho_p u_{ip}\right]\right]\Big/\tilde{\rho}$. The conventional hexahedral finite-volume representation of control-volume-averaged gradients, ∇f, which are computed in accordance with the Gauss-Ostrogradski (Divergence) theorem, $\dfrac{\sum_{\gamma=1,6} f d\mathbf{n}^{\gamma}}{V}$ is noted. The mixture density is defined as $\tilde{\rho} = s\rho + \left(1-s\right)\sum_{p=1}^{N}\rho_p$. N is the number of particles per cell volume, and N_γ denotes the number of particles crossing the cell face in the direction of the area normal $d\mathbf{n}^{\gamma}$, δt represents the change of each quantity over one time step. F_{ip}^{MD} refers to the MD particle force exerted on each particle. The continuum force, $F_i = \nabla_j(\bar{\Pi}_{ij} + \tilde{\Pi}_{ij})$

includes both the deterministic and stochastic continuum Reynolds stress forces in accordance with the Landau-Lifshitz Fluctuating Hydrodynamic (LL-FH) model[2], where the amplitude of thermal fluctuations is inversely proportional to the square root of the continuum hydrodynamics integration time step Δt_{FH} and control volume size, V and also linearly proportional to the square root of the thermodynamic temperature, T, which is equal to the target temperature of the MD ensemble, T_0. For isothermal processes of interest in this work, an isothermal Equation of State (EoS), $p = p(\rho, T_0)$ is assumed, which relates thermodynamic pressure and density of the continuum phase, and which is calibrated from a separate all-atom equilibrium MD simulation of SPC/E water. In the current work, the calibrated EoS can be expressed as $p = \rho(a\rho + b) + \mathrm{c}$, and the simulation parameters including MD details are summarised in Table 1.

The source and sink terms, J_1 and J_2, which determine the phase interaction are defined so that the residuals corresponding to the differences of the cell-averaged particle density and momenta from the same of the two-phase mixture, $\rho' = \tilde{\rho} - \sum_{p=1}^{N} \rho_p$ and $q_i' = \tilde{\rho}\tilde{u}_i - \sum_{p=1}^{N} \rho_p u_{ip}$, are forced to decay to zero (or, at least, stay bounded) to avoid the unwanted phase separation, in accordance with the additional relations:

$$\frac{\delta_t \rho'}{\delta t} + \frac{1}{V}\sum_{\gamma=1}^{6}\left(\rho' \tilde{u}_i \cdot dn_i^{\gamma}\right) = -\alpha \cdot s(1-s)\left(\tilde{\rho} - \sum_{p=1}^{N}\rho_p\right), \tag{5}$$

$$\frac{\delta_t q_i'}{\delta t} + \frac{1}{V}\sum_{\gamma=1}^{6}\left(q_i' \tilde{u}_j \cdot dn_j^{\gamma}\right) = -\beta s(1-s)\left(\tilde{\rho}\tilde{u}_i - \sum_{p=1}^{N}\rho_p u_{ip}\right), \; i, j = 1, 2, 3 \tag{6}$$

Accordingly, to satisfy the conservation of particle mass and momentum equations,

$$\frac{\delta_t\left(\sum_{p=1}^{N} m_p\right)}{\delta t} + \sum_{\gamma=1}^{6}\left[\left(\sum_{p=1}^{N_\gamma}\frac{d\mathbf{x}_p}{dt}\rho_p\right)d\mathbf{n}^{\gamma}\right] = 0 \text{ and} \tag{7}$$

$$\delta_t\left(\sum_{p=1}^{N} m_p u_{ip}\right)+\sum_{\gamma=1}^{6}\left[\left(\sum_{p=1}^{N_\gamma}\frac{d\mathbf{x}_p}{dt}\rho_p u_{ip}\right)d\mathbf{n}^\gamma\right]\cdot\delta t=\sum_{p=1}^{N}\left[m_p\frac{du_{ip}}{dt}\right]\cdot\delta t\,, \tag{8}$$

the molecular dynamics equations are modified to

$$\frac{dx_{ip}}{dt}=(1-s_p)u_{ip}+s_p\tilde{u}_{ip}+\alpha s_p(1-s_p)\frac{\partial\rho'}{\partial x_i}\Bigg/\sum_{p=1}^{N}\rho_p \tag{9}$$

and

$$\frac{du_{jp}}{dt}=(1-s_p)F_{jp}^{MD}\Big/\rho_p+s_pF_{jp}\Big/\sum_{p=1}^{N}\rho_p+\left[\frac{\partial}{\partial x_i}\left(\frac{\sum_{p=1}^{N}\left[\alpha s_p\left(1-s_p\right)u_{jp}\rho_p\frac{\partial\rho'}{\partial x_i}\right]}{\sum_{p=1}^{N}\rho_p}\right)\right]_p\Bigg/\sum_{p=1}^{N}\rho_p+$$
$$\left[\beta s\left(1-s\right)q_j'\right]_p\Big/\sum_{p=1}^{N}\rho_p \tag{10}$$

where i, j = 1,2,3 are Cartesian coordinate components, p is the particle sub-index which refers to the point/ field value defined/interpolated to the particle location, and $\alpha,\beta>0$ are adjustable coupling constants, which are obtained from the model calibration by comparison with the all-atom MD simulations in the equilibrium case.

For numerical solution of equations (1) – (4), following Ref.[21], new dependent variables $\rho^*=\tilde{\rho}-\rho'$ and $q_i=\tilde{u}_i\tilde{\rho}-q_i'$ are introduced to re-arrange the equations to the so-called Generalised Landau-Lifshitz Fluctuating Hydrodynamics (GLL-FH) form, which is a single phase formulation of the original two-phase-like equations (1)-(4),

$$\frac{\delta_t\rho^*}{\delta t}+\frac{1}{V}\sum_{\gamma=1}^{6}\left[s\rho^*\tilde{u}_i\cdot dn_i^\gamma\right]=Q_\rho+\alpha s(1-\mathrm{s})\cdot\rho' \tag{11}$$

$$\frac{\delta_t q_i}{\delta t}+\frac{1}{V}\sum_{\gamma=1}^{6}\left[sq_i\tilde{u}_j\cdot dn_j^\gamma\right]=Q_i+sF_i+\beta s(1-\mathrm{s})\cdot q_i'\;\; i, j=1, 2, 3. \tag{12}$$

where the right-hand-side terms account for the control-volume-averaged mass and momentum terms sources corresponding to the feedback from the MD particles to the continuum hydrodynamics phase,

$$Q_\rho=-\frac{1}{V}\sum_{\gamma=1}^{6}\left[\left(\sum_{p=1}^{N_\gamma}\left(1-s_p\right)u_{ip}\rho_p\right)dn_i^\gamma\right] \tag{13}$$

and

$$Q_i = \sum_{p=1}^{N}\left[\left(1-s_p\right)F_{ip}^{\ MD}\right] - \frac{1}{V}\sum_{\gamma=1}^{6}\left[\sum_{p=1}^{N_\gamma}\left(\left(1-s_p\right)u_{jp}\rho_p u_{ip}\right)dn_j^\gamma\right] \quad i, j=1, 2, 3. \tag{14}$$

In the actual MD implementation, an additional Langevin dissipative term is included in the MD velocity equation

$$\frac{dx_{ip}}{dt} = u_i^* \tag{15}$$

$$\frac{du_{ip}}{dt} = -\gamma u_{ip} + F_i^*,\ \gamma = \frac{1-\lambda}{\Delta t_{MD}}, \tag{16}$$

where λ is the rescaling parameter of the Berendsen thermostat [23], $\lambda = \sqrt{1+\frac{\Delta t_{MD}}{\tau}\left(\frac{T_{ref}}{T}-1\right)}$, τ is its characteristic relaxation time, T_{ref} is the target MD temperature, and T is the instantaneous temperature of MD particles for the relevant ensemble averaging. Furthermore, to include the continuum hydrodynamics effect in the multi-resolution domain, the *s*-dependent local thermostat was suggested[22] to partly account for the particle inertia effect,

$$T_{ref} = \frac{1-s}{f\left(s\right)}T_0, \text{ where } f\left(s\right)=(1-s/2). \tag{17}$$

By integrating the MD particle equations, the modified Leapfrog scheme is obtained [22]

$$x_{ip}\left(t+\Delta t\right) = x_{ip}\left(t\right) + u_i^*\frac{\mathrm{e}^{\gamma\Delta t}-1}{\gamma} \tag{18}$$

$$u_{ip}\left(t+\frac{\Delta t}{2}\right) = u_{ip}\left(t-\frac{\Delta t}{2}\right)\mathrm{e}^{-\gamma\Delta t} + F_i^*\frac{\mathrm{e}^{-\gamma\Delta t/2}-\mathrm{e}^{-3\gamma\Delta t}}{\gamma}, \tag{19}$$

$$u_i^* = \frac{dx_{ip}}{dt} = (1-s_p)u_{ip} + s_p\tilde{u}_{ip} + \alpha s_p(1-s_p)\frac{\partial\rho'}{\partial x_i}\Big/\sum_{p=1}^{N}\rho_p\ ,$$

where

$$F_j^* = (1-s_p)F_{jp}^{MD}\Big/\rho_p + s_p F_{jp}\Big/\sum_{p=1}^{N}\rho_p + \left[\frac{\partial}{\partial x_i}\left(\frac{\sum_{p=1}^{N}\left[\alpha s_p\left(1-s_p\right)u_{jp}\rho_p\frac{\partial\rho'}{\partial x_i}\right]}{\sum_{p=1}^{N}\rho_p}\right)\right]\Big/\sum_{p=1}^{N}\rho_p \qquad (20)$$

$$+\left[\beta s(1-s)m_j'\right]\Big/\sum_{p=1}^{N}\rho_p$$

This will lead to the corresponding modification of the momentum source term of the GLL-FH equations in comparison with (14),

$$Q_i = \sum_{p=1}^{N}\left[\left(1-s_p\right)F_{ip}^{\ MD}\right] - \frac{1}{V}\sum_{\gamma=1}^{6}\left[\sum_{p=1}^{N_\gamma}\left(\left(1-s_p\right)u_{jp}\rho_p u_{ip}\right)dn_j^\gamma\right] - \gamma\sum_{p=1}^{N}u_{ip}\rho_p \qquad (14a)$$

2.2 Application to the Poiseuille flow: the linearisation approach and the computational method

To enforce a non-uniform background incompressible flow, $\left(\rho_0, \boldsymbol{u_0}\left(\boldsymbol{x}\right)\right)$, a linearization algorithm is introduced as follows.

The GLL-FH solution is considered as a linear superposition of the steady solution and the unsteady fluctuation, $(\tilde{\rho},\tilde{\boldsymbol{u}}) = (\rho_0 + \rho''(\boldsymbol{x},t), \boldsymbol{u_0}(\boldsymbol{x}) + \boldsymbol{u}''(\boldsymbol{x},t))$, where the double prime denotes the thermal fluctuation. Such linearization reduces the problem to (i) the solution of the governing GLL-FH equations (11) and (12) for density and thermal velocity fluctuation, $\left(\tilde{\rho}, \boldsymbol{u}''(\boldsymbol{x},t)\right)$ under the simplified periodic boundary conditions and (ii) the determination of the background flow solution $\left(\rho_0, \boldsymbol{u_0}\left(\boldsymbol{x}\right)\right)$. Notably, the latter can be obtained from a separate continuum flow calculation or specified analytically, as in the case of the Poiseuille flow case considered in the numerical example section. The MD equations (18)-(20) are solved with the full reconstructed solution $(\tilde{\rho},\tilde{\boldsymbol{u}})$. Hence, for consistency, the MD velocities appearing in the source term Q_i (14a) are redefined to subtract the mean values, $u_{ip} \equiv u_{ip} - \frac{1}{N}\sum_{p=1}^{N}u_{ip}$.

It can be noted that the GLL-FH equations are solved for the velocity fluctuation variable consistently with MD equations. In accordance with this formulation, the non-uniform

background flow is included separately and, thereby, is not affected by the Langevin dissipation. Due to the linearisation approach, the non-uniform macroscopic flow is preserved and the total linear momentum conservation property is not violated. A more general approach to enforce the total momentum conservation would be to use Dissipative Particle Dynamics (DPD) thermostat, which is based on the relative velocity between a pair of interacting particles. Once implemented in future work, such approach would not require using the suggested linearisation method to conserve the bulk flow momentum.

Following Ref.[22], the GLL-FH equations (5),(6), (11)-(13), (18)-(20) are solved by a predictor-corrector scheme, where the Eulerian part of the model (5),(6), (11)-(13) is solved by a central finite-volume method on a uniform computational grid of control volumes V. The integration time step of the control-volume-averaged equations, Δt_{FH} is 10 times larger in comparison with the MD time step, Δt_{MD}. In the two-way coupled solution, the hydrodynamic fields are driven by the collective dynamics of MD particles while coordinates and velocities of the MD particles are concurrently updated in accordance with (18)-(20).

Most details of the implemented numerical algorithm are identical to the algorithm published in Ref.[22]. Two modifications to increase the stability of the numerical scheme for solving the GLL-FH equations are summarised below.

First, the modified version of equations (5) and (6) is solved by re-arranging the source term to include the evolutionary variable in the dissipation terms thereby enabling an improved stability,

$$\frac{\delta_t \rho'}{\delta t} + \frac{1}{V}\sum_{\gamma=1}^{6}\left(\rho' \tilde{u}_i \cdot dn_i^{\gamma}\right) = -\frac{1}{2}\alpha \cdot s(1-s)\left(\tilde{\rho} - \sum_{p=1}^{N}\rho_p\right) - \frac{1}{2}\alpha \cdot s(1-s)\rho' \tag{5a}$$

$$\frac{\delta_t q_i'}{\delta t} + \frac{1}{V}\sum_{\gamma=1}^{6}\left(q_i' \tilde{u}_j \cdot dn_j^{\gamma}\right) = -\frac{1}{2}\beta s(1-s)\left(\tilde{\rho}\tilde{u}_i - \sum_{p=1}^{N}\rho_p u_{ip}\right) - \frac{1}{2}\beta s(1-s) q' \text{ , } i, j = 1, 2, 3 \tag{6a}$$

Secondly, for more accurate approximation of the ensemble-averaged MD forces $\sum_{p=1}^{N}\left[\left(1-s_p\right)F_{ip}^{\ MD}\right]$ of the momentum source term Q_i in (14a), an improved averaging procedure is implemented. The MD forces are driven by steep MD pair potentials. Without a sufficient ensemble averaging, the force term has a highly oscillatory behaviour, which may lead to numerical instability when solving the GLL-FH equations. Hence, to compensate for a limited time averaging, the MD force term is spatially filtered by averaging over a super-control volume of 3^3 cells, where the central cell corresponds to the current control volume of interest (Figure 1).

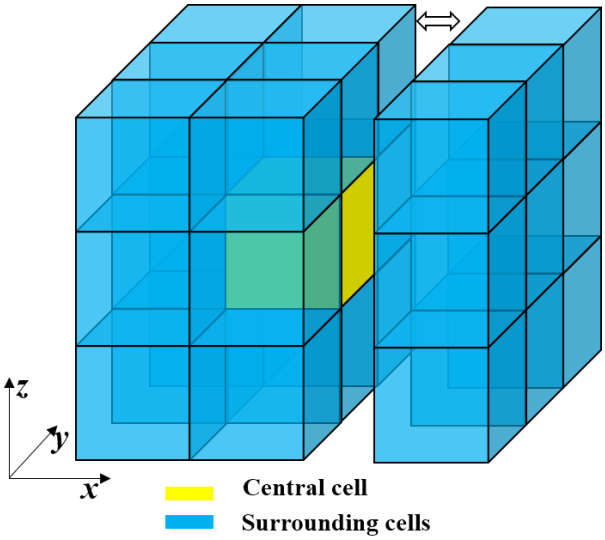

Figure 1. Schematic of a super-control volume comprising 33 cells for calculation of the cell-averaged MD force term in the current central cell.

Following Ref.[22], the computational domain includes a large hydrodynamic box domain, $-L \le x_1, x_2, x_3 \le L$ that overlaps with a small MD particle domain in the center. Continuum hydrodynamic equations (5), (6), (11)-(13) are solved in the large box domain, and the modified MD particle equations (18)-(20) are solved in the particle domain with NVT ensemble. Due to the improved stability, the current implementation of the GLL-FH model permits the testing of different long-range electrostatics methods in the MD part of the multiscale model. Specifically, the implementations of the model based on the Cut-off and Reaction-Field[24] methods in

GROMACS are compared. In addition, we have also implemented the same multiscale model with the Particle-Mesh Ewald (PME) method, which yields similar results to the Reaction-Field, hence, is not discussed separately.

The background flow corresponding to the planar Poiseuille flow is imposed

$$\boldsymbol{u_0}(\boldsymbol{x}) = (u_{01}, 0, 0), u_{01} = U_{\max}\left(1 - \left(\frac{x_2}{L}\right)^2\right) - U_0, \tag{21}$$

where $U_0 = \frac{1}{2L}\int_{-L}^{L} U_{\max}\left(1 - \left(\frac{x_2}{L}\right)^2\right) \mathrm{d}x_2$ corresponds to the shift applied to subtract the center of mass velocity in order to simplify the simulation in GROMACS. For the current test, $U_{\max} = 0.05$ nm·ps^{-1} and $L \equiv$ box domain length with 9×9×9 elementary control volumes are considered.

To investigate the effect of the size of the hydrodynamic computational domains, two computational domains, which correspond to 9×9×9 and 17×17×17 elementary control volumes are considered. The MD particle domain in the centre of the hydrodynamic box domain corresponds to 5×5×5 control volumes of the full grid. On average, each elementary control volume in the particle domain contains 243 water molecules at the normal atmospheric pressure (1 bar) and room temperature conditions (298.15 K). Periodic boundary conditions are used for both the hydrodynamic box and the interior MD particle domains. Together with considering of the Cut-off and Reaction-Field methods for the long-range MD interactions this amounts to 4 cases (2 domains × 2 models) to be tested.

To complete the hybrid model description, the s-function, which delineates the regions of the atomistic resolution from the hydrodynamics region is specified following Ref.[21] and Ref.[22] so that it is spherically distributed with the radial distance from the centre, $r = \sqrt{x_1^2 + x_2^2 + x_3^2}$ inside the particle domain

$$s(r)=\begin{cases}0, & r \le R_{MD} \\ \dfrac{r-R_{MD}}{R_{FH}-R_{MD}} S_{\max}, & R_{MD} < r < R_{FH} \\ S_{\max}, & r \ge R_{FH}\end{cases}, \tag{22}$$

and is set to 1 in the hydrodynamics box domain outside of the MD region.

Parameters of the suggested model such as S_{max}, R_{MD} and R_{FH} as well as the coupling parameters, α and β are acquired from a suitable calibration of the model for the equilibrium water simulation case. Summary of the model parameters is provided in Table 1.

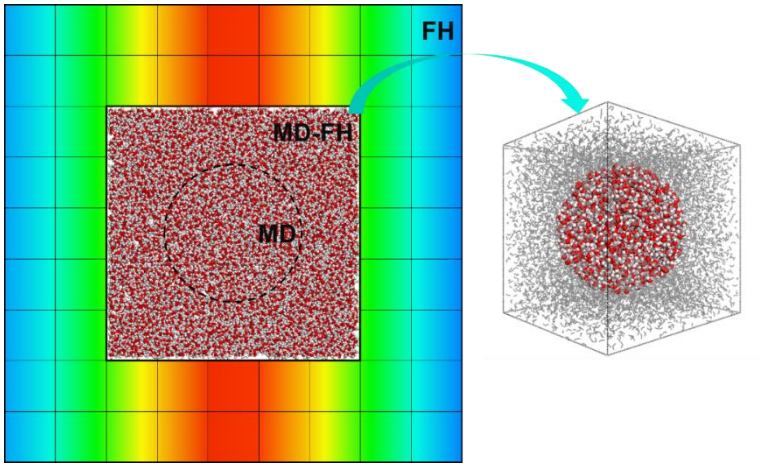

Figure 2. Computational setup for the simulation of water fluctuations: the overlapping continuum and particle box domains. The insert shows an outline of the spherical pure MD region (s = 0) inside the MD particle box.

Table 1. Simulation parameters of the GLL-FH model of the SPC/E water flow

Items	value
Number of atoms (molecules)	91125 (30375)
Molecular mass (g·mol^{-1})	18.015
Temperature (K)	298.15
MD box volume (nm^3)	9.686×9.686×9.686
MD time step (ps)	0.001
Continuum solver time step (ps)	0.01
Average density (amu·nm^{-3})	602.18
Shear viscosity (amu·nm^{-1}·ps^{-1})	409.496
Bulk viscosity (amu·nm^{-1}·ps^{-1})	933.41
Maximum concentration of the hydrodynamic phase in the particle domain $S_{\max}$	0.5
Number of control volumes in the MD box domain	5×5×5
Number of control volumes in the continuum box domain	9×9×9&17×17×17
Dimensionless radius of the pure MD zone, $2R_{MD}V^{-1/3}$	0.5

Dimensionless radius of the pure MD/FH zone, $2R_{FH}V^{-1/3}$	1
MD/FH coupling parameters, α (ps^{-1}), β (ps^{-1})	500, 1000
Thermostat relaxation time, (ps)	0.01
Constraints algorithm	SETTLE[25]
Parameters of EoS $p=\rho(a\rho+b)+c$	a=0.010, b=-10.133, c=2428.920

3 Results and discussion

3.1 Flow profiles

Figure 3 compares the time-averaged velocity profiles of FH solutions and MD solutions for all four cases, the Cut-off and Reaction-Field electrostatics methods with two domain sizes, 9×9×9 and 17×17×17 cells. The three solutions compared against the analytical Poiseuille flow solution, u_{01} correspond to the time-averaged velocity profile $\langle \tilde{u}_1 \rangle$ and the time- and cell-volume-averaged profile of the MD particle velocities, $\frac{1}{N}\sum_{p=1}^{N} u_{ip}$ in the full particle zone including the buffer region and in the pure MD zone only. In all cases, the numerical solutions closely capture the analytical Poiseuille flow profile. It can be seen the MD velocity solutions of the large computational domain are less sensitive to the choice of the electrostatics interaction modelling. For the smaller domain, the Reaction-Field method leads to a less noisy and more accurate solution of the velocity profile. The larger sensitivity of the plain Cut-off method can be explained by the fact that it cannot accurately describe the long-range dipole-dipole interactions.

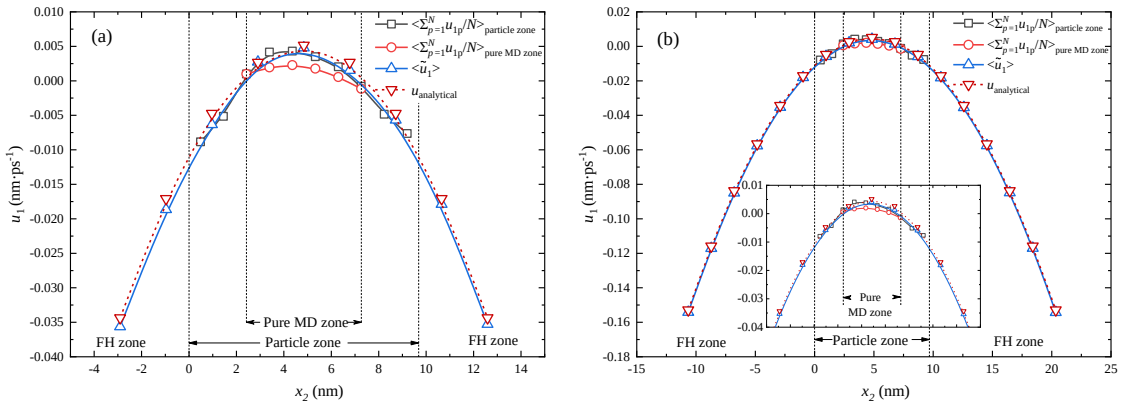

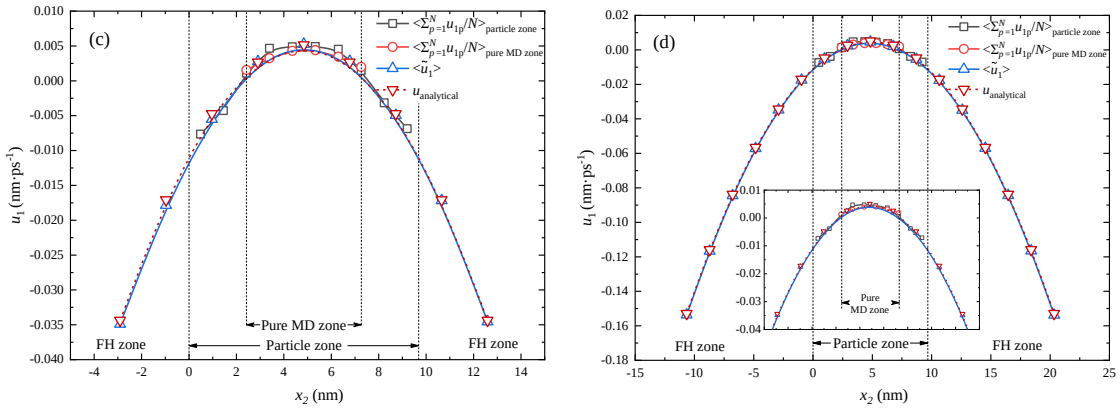

Figure 3. Time-averaged flow velocity profiles of the continuum field and MD particle solutions for different hydrodynamic box sizes and MD electrostatics methods: (a) Cut-off method in the 9×9×9 domain, (b) Cut-off method in the 17×17×17 domain, (c) Reaction-field method in the 9×9×9 domain, and (d) Reaction-field method in the 17×17×17 domain.

3.2 Thermal fluctuations

The computed standard deviations of density and velocity fluctuations of the MD phase and the hydrodynamics fields, $(\rho'', \boldsymbol{u}'')$ of the four solutions are summarised in Tables 2a and b. The MD fluctuations are ensemble-averaged over each control volume V of the MD particle part of the computational domains and compared with the reference analytical solutions. The latter solutions are based on the grand-canonical-ensemble fluctuating hydrodynamics theory, $STD(\rho) = c_T^{-1}\sqrt{\rho k_B \frac{T_0}{V}}$ and $STD(u) = \sqrt{k_B \frac{T_0}{\rho V}}$, where c_T^{-1} is the isothermal speed of sound and k_B is Boltzmann constant.

For all four cases, the standard deviations of the MD particle and continuum fluctuating hydrodynamics solutions are approximately within 15% for density fluctuations and within 10% for velocity fluctuations one from the other. This suggests that the artificial phase separation did not occur, and the phase coupling of two-phase flow analogy method has been consistent.

On the other hand, it can be noted that the thermal fluctuations of density are 30-50% lower than the analytical solution based on the grand canonical ensemble theory. This is explained by the effect of the local thermostat implemented in the buffer region. Indeed, it can be recalled that the *s*-dependent thermostat (17) is set to decrease the reference temperature with increase of the hydrodynamic force contribution (*s* increasing). Hence, when averaged

over the entire MD particle domain, the thermal fluctuations of the particle phase of the GLL-FH are expected to be smaller than the reference analytical solution that also includes the hydrodynamics contribution. In this respect, the solution of the Reaction-Field method appears to be more consistent due to the fact it demonstrates moderately lower fluctuations than the predictions based on the grand canonical ensemble theory, while the Cut-off method tends to overestimate the fluctuations.

Of particular interest are the thermal velocity and density fluctuations in the pure MD region, which corresponds to the region of the highest resolution of the GLL-FH model. Hence, Table 3 shows the standard deviations of effective particle density and particle velocity fluctuations computed in control volume corresponding to the pure MD zone (s=0), without considering the buffer region, where the local thermostat is used, i.e. time averaged $\sqrt{\sum_{p=1}^{N}\left(\rho_p-\frac{\sum_{p=1}^{N}\rho_p}{N}\right)^2\Big/N}$ and $\sqrt{\sum_{p=1}^{N}\left(v_p-\frac{\sum_{p=1}^{N}v_p m_p\Big/V_{cell}}{\sum_{p=1}^{N}m_p\Big/V_{cell}}\right)^2\Big/N}$. It can be seen that in all cases the fluctuations of the hybrid multiscale model are within 0.5% of the solutions of the reference all-atom equilibrium MD simulation of SPC/E water.

Table 2a. Standard deviations of density fluctuations averaged in the complete particle domain domain.

	STD_ρ_{MD} (amu·nm^{-3})	STD_ρ_{FH} (amu·nm^{-3})
Cut-off (FH cells 9×9×9)	6.834	5.768
Reaction-field (FH cells 9×9×9)	8.510	7.202
Cut-off (FH cells 17×17×17)	6.775	5.757
Reaction-field (FH cells 17×17×17)	8.517	7.206
Analytical solution	10.049	

Table 2b. Standard deviations of velocity fluctuations averaged in the complete particle domain.

	$STD\_u_{x\_MD}$ ($nm \cdot ps^{-1}$)	$STD\_u_{y\_MD}$ ($nm \cdot ps^{-1}$)	$STD\_u_{z\_MD}$ ($nm \cdot ps^{-1}$)	$STD\_u_{x\_FH}$ ($nm \cdot ps^{-1}$)	$STD\_u_{y\_FH}$ ($nm \cdot ps^{-1}$)	$STD\_u_{z\_FH}$ ($nm \cdot ps^{-1}$)
Cut-off (FH cells 9×9×9)	0.0235	0.0231	0.0231	0.0254	0.0253	0.0253
Reaction-field (FH cells 9×9×9)	0.0186	0.0181	0.0181	0.0210	0.0210	0.0210
Cut-off (FH cells 17×17×17)	0.02312	0.0229	0.02288	0.02515	0.02534	0.02532
Reaction-field (FH cells 17×17×17)	0.0184	0.0181	0.0181	0.0206	0.0207	0.0207
Analytical solution	0.0238					

Table 3a. Standard deviations of particle density fluctuations in the pure MD domain.

	STD_ρ ($amu \cdot nm^{-3}$)
Cut-off (FH cells 9×9×9)	0.9721
Reaction-field (FH cells 9×9×9)	0.9722
Cut-off (FH cells 17×17×17)	0.9769
Reaction-field (FH cells 17×17×17)	0.9722
Reference all-atom MD solution	0.9721

Table 3b. Standard deviations of particle velocity fluctuations in the pure MD domain.

	STD_u_x ($nm \cdot ps^{-1}$)	STD_u_y ($nm \cdot ps^{-1}$)	STD_u_z ($nm \cdot ps^{-1}$)
Cut-off (FH cells 9×9×9)	0.9588	0.9572	0.9609
Reaction-field (FH cells 9×9×9)	0.9595	0.9601	0.9588
Cut-off (FH cells 17×17×17)	0.9572	0.9610	0.9584
Reaction-field (FH cells 17×17×17)	0.9587	0.9591	0.9599
Reference all-atom MD solution	0.9575	0.9578	0.9576

Figure 4 shows the time history of volume-averaged density and temperature computed in the pure MD zone for the same four cases. Thanks to the local thermostat implemented in the GLL-FH model, the temperature in the pure MD zone is well controlled in all cases. No

influence of the hydrodynamic domain size on the predicted temperature and density signals can be noted.

However, depending on the choice of the method for computing long-range interactions, the mean density calculation shows some variability: the Cut-off method overestimates the cell-averaged water density by about 7.5-8.7% while the reaction-field overestimates by only about 1%. As water is a highly incompressible substance, the 7-8 fold reduced error in density suggests that the Reaction-Field method leads to an improved preservation of the local reference pressure in comparison with the Cut-off method.

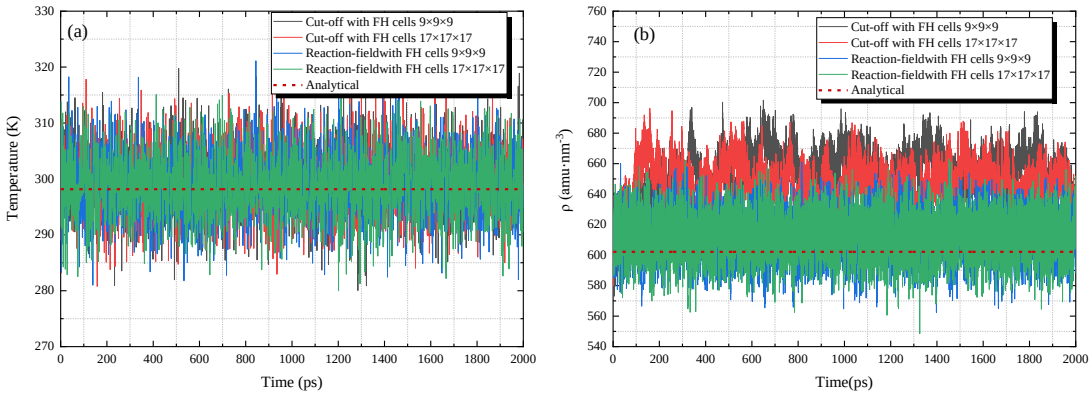

Figure 4. Dependence of the temperature (a) and density (b) in the pure MD region of the computational domain on the domain size and the electrostatics interaction method: Cut-off method in the 9×9×9 domain, Cut-off method in the 17×17×17 domain, Reaction-Field method in the 9×9×9 domain, and Reaction-Field method in the 17×17×17 domain.

To complete this sub-section, distributions of the cell-averaged temperature of MD particles along the flow stream-wise, shear-wise, and span-wise directions, which are centred in the pure MD region, are shown in Fig.5. The solutions presented correspond to Reaction-Field method and the 9×9×9 cell computational domain. Other choices of the force field and computational domain sizes lead to very similar temperature distributions, hence, are not included. Fig. 5a shows the particle temperature measured computed from the equipartition theorem. The temperature profiles in all 3 coordinate directions virtually coincide, and the particle temperature in the central pure MD region is equal to the target value, T_0. Fig.5b shows the reconstructed full temperature including the hydrodynamic phase contribution in accordance with Eq.(17). Good agreement with the target temperature T_0 is evident for all spatial locations including the hydrodynamics-dominated regions near the boundaries of the

MD box. This confirms that the implemented local thermostat works well for the non-equilibrium flow problem considered.

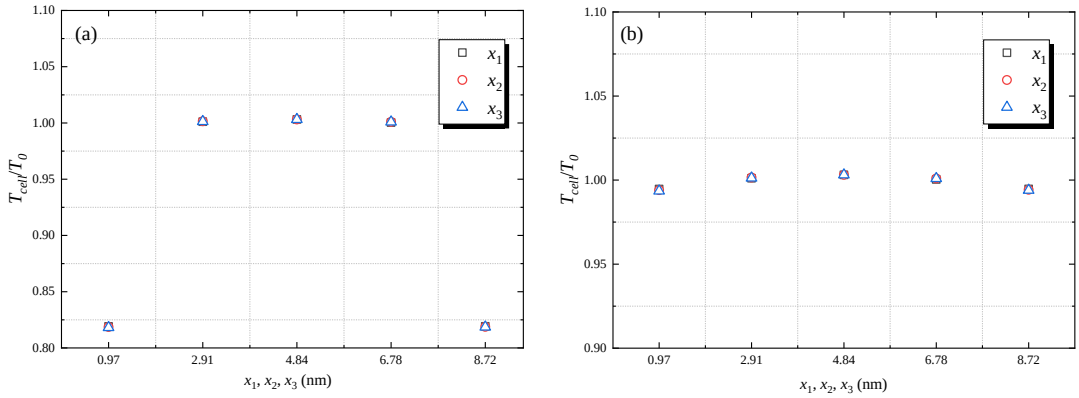

Figure 5. Profiles of the cell-averaged temperature of MD particles along the stream-wise (x_1), shear-wise (x_2), and span-wise (x_3) directions normalised on the target temperature T_0 and computed from (a) the equipartion theorem and (b) the equipartion theorem including the hydrodynamic phase contribution in accordance with Eq.(17). The model corresponds to the Reaction-Field method in the 9×9×9 domain.

3.3 Radial distribution function

The radial distribution function (RDF) is an important indicator showing whether the interatomic forces in water have been accurately reproduced. Hence, RDF of water atoms has been computed in the pure MD region for all 4 GLL-FH models and compared with the reference all-atom equilibrium MD solution. The results for O-O atoms are shown in Figure 6. Again, no influence of the hydrodynamic domain size on the predicted RDF function can be noted. However, it can be observed that the solutions of the Cut-off model correctly capture the first hydration layer and yet smear the subsequent dip associated with repulsion, which is likely to be due to the water density overestimation. In comparison with this, the Reaction-Field models capture both the features of the RDF curve and are in excellent agreement with the reference all-atom MD solution.

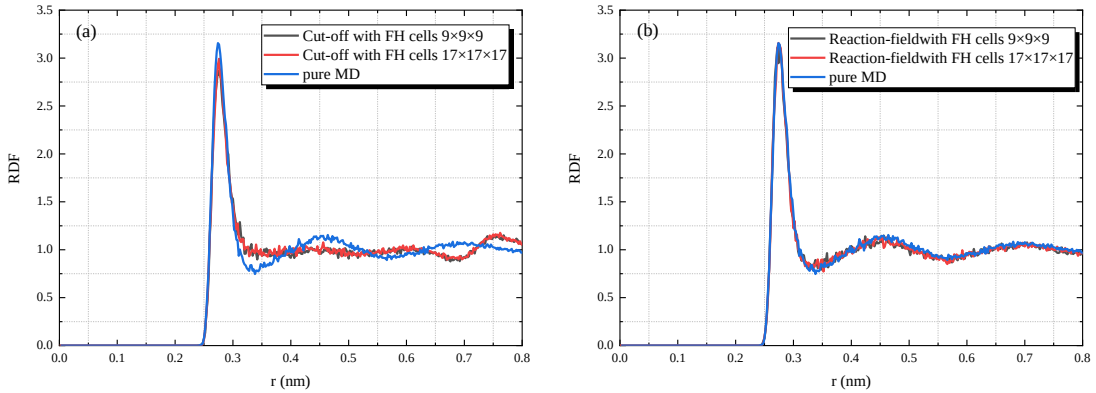

Figure 6. Radial distribution functions of O-O atoms for different electrostatics methods Cut-off method (a) and Reaction-field method(b): Cut-off method in the 9×9×9 domain, Cut-off method in the 17×17×17 domain, Reaction-field method in the 9×9×9 domain and Reaction-field method in the 17×17×17 domain. The reference pure all-atom MD solution is included for comparison.

3.4 Evaluation of computational efficiency

Since hybrid atomistic-scale resolving multiscale methods are considerably more complex in comparison with the single-scale methods like Molecular Dynamics, computational efficiency of the suggested multiscale method is of great interest. All current GLL-FH models have been implemented in GROMACS and run on a workstation computer. The computational cost of the multiscale solution does not depend on the type of the long-range electrostatics method, cut-off and reaction-field and only weakly depends on the size of the hydrodynamics box computational domain. Since the main cost is associated with solving the MD particle equations in the small interior domain, the equivalent cost of equilibrium all-atom MD simulation in the entire computational domain is much greater. The difference in the computational cost of the hybrid multiscale method and the all-atom MD model in the same computational domains, 9×9×9 and 17×17×17 control volumes are summarised in Table 4. Notably, for the smaller computational domain, 9×9×9, the suggested multiscale model is a factor of 4 faster that the all-atom equilibrium MD simulation. For the larger size domain of 17×17×17 volumes, the hybrid method already becomes a factor of 18 faster in comparison with the all-atom simulation. For large problems, the computational benefits of the hybrid

method in comparison with the pure MD method should increase proportionally to the size of the hydrodynamics box simulation domain.

Table 4. Simulation times of the hybrid multiscale method against the all-atom equilibrium molecular dynamics for different computational domains, CPU hours for nanosecond simulated.

Domain size	(9×9×9)	(17×17×17)
CPU hours of the hybrid method /CPU hours of the all-atom MD simulation	5.81/21.24=0.274	7.78/138.34=0.056

4. Conclusions

The thermostat-consistent fully coupled molecular dynamics – generalised fluctuating hydrodynamics model has been extended to non-equilibrium water flow simulations. The key ingredients of this extension are the increased robustness of the method due to the use of a more stable approximation of the source terms in the governing fluctuating hydrodynamics equations and the linearization formulation, which simplifies setting up of the boundary conditions. The strong coupling and improved numerical stability of the hybrid multiscale method allow using the advanced algorithms of modelling of long-range electrostatic interactions in water, such as the Reaction-Field and Particle-Mesh Ewald methods in GROMACS, both of which give similar results.

For validation, the method is applied for a multi-resolution simulation of the periodic Poiseuille flow of SPC/E water. It is shown that the time-averaged flow velocity profile compares well with the analytical solution, the thermal density and velocity fluctuations are within the expected tolerance from the theoretical predictions of the grand canonical ensemble fluctuating hydrodynamics theory, and the fluctuations in the pure molecular dynamics region are within 0.5% from the reference all-atom molecular dynamics simulation. **In addition, distributions of the cell-averaged temperature of MD particles along the flow stream-wise, shear-wise, and span-wise directions are shown to be in good agreement with the target temperature value in all spatial locations including those dominated by hydrodynamics.**

It is shown that the solution based on the Reaction-Field method captures both the mean temperature and density in the atomistic region of the hybrid model within 1% from the specified conditions and captures well both the hydration layer peak and the subsequent deep of the RDF function.

The computational efficiency of the non-equilibrium fully coupled molecular dynamics – generalised fluctuating hydrodynamics model is similar to the previously reported equilibrium version of the same model: it is a factor of 4 to 18 faster compared to the all-atom equilibrium molecular dynamics model depending on the overall domain size. The current implementation in the popular open-source code such as GROMACS makes the suggested model available to other researchers working in the area of atomistic scale resolving simulations of non-equilibrium flows.

Code availability

The multiscale code with all parameter files and README can be downloaded following the GitHub link: https://github.com/ikorotkin/gromacs_fhmd-langevin_non-equilibrium

Acknowledgements

The work of XL was supported by the China Scholarship Council (CSC) and Postgraduate Research & Practice Innovation Program of Jiangsu Province, Grant No. KYCX21_2174. IK and SK gratefully acknowledge the funding under the European Commission Marie Skłodowska-Curie Individual Fellowship Grant No. H2020-MSCA-IF-2015-700276 (HIPPOGRIFFE). The work was also supported by European Commission in the framework of the RISE program, Grant No. H2020-MSCA-RISE-2018-824022-ATM2BT and the National Natural Science Foundation of China, Grant No.51776218.

Received: ((will be filled in by the editorial staff))
Revised: ((will be filled in by the editorial staff))
Published online: ((will be filled in by the editorial staff))

References

[1] O'connell, S. T.; Thompson, P. A., *Phys. Rev. E* **1995,** *52* (6), R5792.

[2] Landau, L. D.; Lifshitz, E. M., *Statistical Physics , Part 1*. Elsevier, Amsterdam: 1980; Vol. 5.

[3] De Fabritiis, G.; Delgado-Buscalioni, R.; Coveney, P., *Phys. Rev. Lett.* **2006,** *97* (13), 134501.

[4] De Fabritiis, G.; Serrano, M.; Delgado-Buscalioni, R.; Coveney, P., *Phys. Rev. E* **2007,** *75* (2), 026307.

[5] Voulgarakis, N. K.; Chu, J.-W., *J. Chem. Phys.* **2009,** *130* (13), 04B605.

[6] Nie, X.; Chen, S.; Robbins, M., *J. Fluid Mech.* **2004,** *500*, 55.

[7] Praprotnik, M.; Delle Site, L.; Kremer, K., *J. Chem. Phys.* **2005,** *123* (22), 224106.

[8] Delgado-Buscalioni, R.; Kremer, K.; Praprotnik, M., *J. Chem. Phys.* **2008,** *128* (11), 114110.

[9] Delle Site, L.; Praprotnik, M.; Bell, J. B.; Klein, R., *Adv. Theory Simul.* **2020,** *3* (5), 1900232.

[10] Markesteijn, A. P.; Karabasov, S. A.; Glotov, V. Y.; Goloviznin, V. M., *Comput. Methods Appl. Mech. Eng.* **2014,** *281*, 29-53.

[11] Pavlov, E.; Taiji, M.; Scukins, A.; Markesteijn, A.; Karabasov, S.; Nerukh, D., *Faraday Discuss.* **2014,** *169*, 285-302.

[12] Korotkin, I.; Nerukh, D.; Tarasova, E.; Farafonov, V.; Karabasov, S., *J. Comput. Sci.* **2016,** *17*, 446-456.

[13] Korotkin, I.; Karabasov, S.; Nerukh, D.; Markesteijn, A.; Scukins, A.; Farafonov, V.; Pavlov, E., *J. Chem. Phys.* **2015,** *143* (1), 014110.

[14] Hu, J.; Korotkin, I.; Karabasov, S., *J. Chem. Phys.* **2018,** *149* (8), 084108.

[15] Hu, J.; Korotkin, I.; Karabasov, S., *J. Mol. Liq.* **2019,** *280*, 285-297.

[16] Li, F.; Korotkin, I.; Farafonov, V.; Karabasov, S. A., *J. Mol. Liq.* **2021,** *337*, 116111.

[17] Tarasova, E.; Korotkin, I.; Farafonov, V.; Karabasov, S.; Nerukh, D., *J. Mol. Liq.* **2017,** *245*, 109-114.

[18] Li, F.; Korotkin, I.; Taiji, M.; Karabasov, S., **2020,** *DOI: 10.13140/RG.2.2.14247.57763*.

[19] Scukins, A.; Nerukh, D.; Pavlov, E.; Karabasov, S.; Markesteijn, A., *Eur. Phys. J.: Spec. Top.* **2015,** *224* (12), 2217-2238.

[20] Van Der Spoel, D.; Lindahl, E.; Hess, B.; Groenhof, G.; Mark, A. E.; Berendsen, H. J., *J. Comput. Chem.* **2005,** *26* (16), 1701-1718.

[21] Korotkin, I.; Karabasov, S., *J. Chem. Phys.* **2018,** *149* (24), 244101.

[22] Liu, X.; Korotkin, I.; Rao, Z.; Karabasov, S., *Adv. Theory Simul.* **2021,** *4* (4), 2000209.

[23] Berendsen, H. J.; Postma, J. v.; van Gunsteren, W. F.; DiNola, A.; Haak, J. R., *J. Chem. Phys.* **1984,** *81* (8), 3684-3690.

[24] Barker, J. A.; Watts, R. O., *Mol. Phys.* **1973,** *26* (3), 789-792.

[25] Miyamoto, S.; Kollman, P. A., *J. Comput. Chem.* **1992,** *13* (8), 952-962.